PHYSICAL REVIEW B **66**, 085312 (2002)

Strain-induced semimetal-semiconductor transition in InAs/GaSb broken-gap quantum wells

A. Zakharova
Institute of Physics and Technology of the Russian Academy of Sciences, Nakhimovskii Avenue 34, Moscow 117218, Russia

S. T. Yen
Department of Electronics Engineering, National Chiao Tung University, Hsinchu, Taiwan, Republic of China

K. A. Chao
Department of Physics, Lund University, Sölvegutun 14A, S 233 62 Lund, Sweden
(Received 01 March 2002; published 15 August 2002)

We investigate the hybridization of the electron, heavy-hole and/or light-hole dispersion relations in strained InAs/GaSb quantum wells. In the considered structures, the lowest electron level lies below several hole levels at zero in-plane wave vector $\mathbf{k}_{\parallel}$, so that the anticrossings of subbands produce gaps in the in-plane dispersions. To calculate the electronic band structures of such quantum wells grown on different substrates, we use the eight-band $\mathbf{k}\cdot\mathbf{p}$ model and the scattering matrix method. We have found that the order of levels at the zone center ($\mathbf{k}_{\parallel}=0$), gap positions and magnitudes can change due to the lattice-mismatched strain. Strain can also enhance the hybridization of electron and light-hole states at $\mathbf{k}_{\parallel}=0$ considerably. In the structure with a thick InAs layer grown on GaSb, we have obtained a negative indirect gap in the in-plane dispersion resulting from the anticrossing of electronlike and highest heavy-hole-like subbands. If the substrate is InAs, the gap becomes direct and positive. This phenomenon can be treated as strain-induced semimetal-semiconductor phase transition.

DOI: 10.1103/PhysRevB.66.085312 PACS number(s): 73.21.Ac, 73.21.Fg

I. INTRODUCTION

An interesting characteristic feature of broken-gap heterostructures made from InAs, GaSb, AlSb is that the valence band maximum of GaSb lies above the conduction band minimum of InAs. Because of this the electrons can move across an InAs/GaSb interface from the valence band of GaSb to the conduction band of InAs, leading to a semimetallic phase where electrons in InAs coexist with holes in GaSb.[1] This phase can be observed in InAs/GaSb superlattices or InAs/GaSb quantum wells sandwiched by AlSb barriers if the InAs and GaSb layers are sufficiently thick, so that the lowest electron spatially quantized level in InAs lies lower than the highest heavy-hole level in GaSb at the zone center. In this case, however, the electron and heavy-hole dispersion curves anticross at $\mathbf{k}_{\parallel}\neq 0$ resulting in a small hybridization gap in the in-plane dispersion predicted by Altarelli.[2] This gap, which has been observed experimentally,[3–7] causes the semicondicting behavior rather than the semimetallic behavior. A number of earlier experiments,[8–12] nevertheless, suggests a semiconductor-semimetal phase transition with the InAs and GaSb layer thickness increasing. Since no negative indirect gap was found in first theoretical investigations,[2,13,14] it was supposed that doping and temperature effects are responsible for the observation of semimetallic phase.

Recently, in parallel with experimental discovery of hybridization of electron and hole levels,[3–7,15] the interest to the theoretical study of this effect in InAs/GaSb superlattices[6,16,17] and InAs/GaSb quantum wells[18–23] was resumed. It has been found that the hybridized electron-hole dispersions are sensitive to both the InAs and the GaSb layer thicknesses. Considerable spin splitting of subbands, resulting from the lack of inversion symmetry and strong spin-orbit interaction, was detected.[17,21–23] The gap positions and magnitudes also depend on the spin orientation of two-dimensional hybridized quasiparticles and the structure parameters. In addition, the gap positions in energy and $\mathbf{k}_{\parallel}$ are different for different directions of in-plane wave vector.[17,21] This anysotropy is especially noticeable for the structures with a thick InAs layer and a thick GaSb layer. Due to the asymmetric dispersion, the structure can exhibit semimetallic behavior, if the gaps at different $\mathbf{k}_{\parallel}$ points do not overlap. When the lowest electron level in InAs is close to the light-hole level in GaSb at $\mathbf{k}_{\parallel}=0$ in the InAs/GaSb quantum well, a considerable hybridization of the zone-center electron and light-hole states occurs, and their wave functions spread over the entire quantum well structure.[22] If the electron level at $\mathbf{k}_{\parallel}=0$ becomes below the light-hole level with the layers of the structure increasing, the electronlike and light-hole-like subbands anticross at some nonzero wave vector $\mathbf{k}_{\parallel}\neq 0$, producing a wide hybridization gap between the two subbands.[23] In this case, several heavy-hole levels are also above the electron level at $\mathbf{k}_{\parallel}=0$, and multiple anticrossings produce multiple minigaps.[17,23] In a thicker layer structure, the two lowest electron levels can lie lower than the highest heavy-hole level at the zone center. Since the hybridization gaps resulting from the mixing of the heavy-hole subband with the two electron subbands occur at different values of energy and $\mathbf{k}_{\parallel}$, such a structure exhibits a semimetallic behavior as shown in Ref. 20.

In this paper we consider the influence of lattice-mismatched strain on electronic band structure of InAs/GaSb quantum wells using Burt's envelope function theory.[24] Since the difference between the lattice constants of InAs and GaSb is less than 1%, this effect has been neglected in all

 ©2002 The American Physical Society

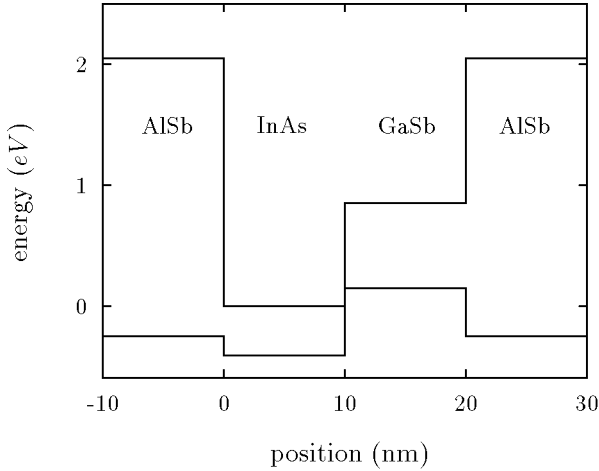

FIG. 1. Conduction and valence band diagram of the AlSb/InAs/GaSb/AlSb broken-gap quantum well structure.

previous investigations of hybridized electron-hole subbands. Nevertheless, such a small difference can produce a noticeable shift in the level and the hybridization gap position. We will show that the order of subbands at the zone center can change because of the lattice-mismatched strain. When the electron level is close to the light-hole level at the zone center, the strain can enhance the hybridization of the electron and light-hole states considerably. In the thicker layer structure grown on GaSb, we found indirect negative hybridization gap between the electronlike and the highest heavy-hole-like subbands due to no overlap of minigaps at different in-plane wave vectors. This indicates the semimetallic properties. In a similar structure grown on InAs, we obtained a direct positive gap resulting in the semiconducting behavior. This difference causes the possibility of strain-induced semimetal-semiconductor phase transition.

We will add to the eight-band $\mathbf{k}\cdot\mathbf{p}$ Burt's model for zinc blende crystals described in Ref. 25 the strain-dependent terms to obtain the solutions for the wave functions in each layer of the structure. Then the eigenvalue problem is solved using the boundary conditions at the interfaces and the scattering matrix algorithm[26] mentioned in Ref. 23. Contrary to the commonly used transfer matrix method, which treats the growing and decaying waves identically that results in the loss of accuracy during computation, the scattering matrix method remains stable even for thick structures and large basis sets in the model used. We describe our model in Sec. II and the method for the solution of eigenvalue problem in Sec. III. In Sec. IV, we present numerical results and discussion. Section V gives a summary.

II. THEORETICAL MODEL

Consider a structure consisting of an InAs/GaSb quantum well sandwiched by two AlSb barriers grown along the [001] direction. This direction is defined as the z axis. We also choose the x axis to be along [100] and the y axis to be along [010]. The band diagram of an InAs/GaSb quantum well structure is shown in Fig. 1. Using the following basis functions:

$$S\uparrow, X\uparrow, Y\uparrow, Z\uparrow, S\downarrow, X\downarrow, Y\downarrow, Z\downarrow, \tag{1}$$

the 8×8 $\mathbf{k}\cdot\mathbf{p}$ Burt's Hamiltonian for the Γ point of zinc blende crystals can be written as[25]

$$\hat{H}=\begin{pmatrix} \hat{H}_4 & 0 \\ 0 & \hat{H}_4 \end{pmatrix}+\hat{H}_{\mathrm{SO}}+\hat{H}_{\epsilon}, \tag{2}$$

where $\hat{H}_4$ is the $\mathbf{k}$-dependent 4×4 block, $\hat{H}_{\mathrm{SO}}$ is the spin-orbit interaction term, and the term $\hat{H}_{\epsilon}$, which we added to the Hamiltonian in Ref. 25, describes the effect of strain on the electronic band structure. The block $\hat{H}_4$ has the following form:

$$\hat{H}_4=\begin{pmatrix} \hat{H}_{cc} & \hat{H}_{cv} \\ \hat{H}_{vc} & \hat{H}_{vv} \end{pmatrix}, \tag{3}$$

where

$$\hat{H}_{cc}=E_c(z)+\hat{\mathbf{k}}A_c(z)\hat{\mathbf{k}}, \tag{4}$$

$$\hat{H}_{cv}=\hat{H}_{vc}^{\dagger}=(iP\hat{k}_x \quad iP\hat{k}_y \quad iP\hat{k}_z), \tag{5}$$

and

$$\hat{H}_{vv}=\begin{pmatrix} \hat{H}_{XX} & \hat{H}_{XY} & \hat{H}_{XZ} \\ \hat{H}_{YX} & \hat{H}_{YY} & \hat{H}_{YZ} \\ \hat{H}_{ZX} & \hat{H}_{ZY} & \hat{H}_{ZZ} \end{pmatrix}. \tag{6}$$

Here $E_c(z)$ is the conduction band edge, $A_c(z)$ reflects the effect of remote bands on the electron effective mass, and P is the interband momentum matrix element. The diagonal and off-diagonal elements of the matrix $\hat{H}_{vv}$ have the following typical forms:

$$\hat{H}_{XX}=E_v(z)-\frac{\Delta}{3}+\hat{k}_xL\hat{k}_x+\hat{k}_yM\hat{k}_y+\hat{k}_zM\hat{k}_z,$$

$$\hat{H}_{XY}=\hat{k}_xN_+\hat{k}_y+\hat{k}_yN_-\hat{k}_x, \tag{7}$$

where $E_v(z)$ is the valence band edge and $\Delta(z)$ is the split-off energy. The parameters M, L, N_+, and N_- are given by

$$L=-(\hbar^2/2m_0)(\gamma_1+4\gamma_2), \tag{8a}$$

$$M=-(\hbar^2/2m_0)(\gamma_1-2\gamma_2), \tag{8b}$$

$$N_-=M-\hbar^2/2m_0, \tag{8c}$$

$$N_+=-(\hbar^2/2m_0)(6\gamma_3)-N_-, \tag{8d}$$

where m_0 is the free electron mass and γ_1, γ_2, and γ_3 are the modified Luttinger parameters. In a heterostructure the parameters M, L, N_+, and N_- are functions of z. Hence the correct order of momentum operators with respect to these parameters given by Eq. (7) is important.

The operator H_{SO} has the form

$$\hat{H}_{SO} = -\frac{\Delta(z)}{3} \times \begin{pmatrix} 0 & 0 & 0 & 0 & 0 & 0 & 0 & 0 \\ 0 & 0 & i & 0 & 0 & 0 & 0 & -1 \\ 0 & -i & 0 & 0 & 0 & 0 & 0 & i \\ 0 & 0 & 0 & 0 & 0 & 1 & -i & 0 \\ 0 & 0 & 0 & 0 & 0 & 0 & 0 & 0 \\ 0 & 0 & 0 & 1 & 0 & 0 & -i & 0 \\ 0 & 0 & 0 & i & 0 & i & 0 & 0 \\ 0 & -1 & -i & 0 & 0 & 0 & 0 & 0 \end{pmatrix}. \tag{9}$$

The term $\hat{H}_\epsilon$ can be expressed as[27]

$$\hat{H}_\epsilon = \begin{pmatrix} \hat{H}_{\epsilon 0} & 0 \\ 0 & \hat{H}_{\epsilon 0} \end{pmatrix}, \tag{10}$$

where the 4×4 block $\hat{H}_{\epsilon 0}$ is

$$\hat{H}_{\epsilon 0} = \begin{pmatrix} a_c\epsilon & 0 & 0 & 0 \\ 0 & h_{xx} & n\epsilon_{xy} & n\epsilon_{xz} \\ 0 & n\epsilon_{yx} & h_{yy} & n\epsilon_{yz} \\ 0 & n\epsilon_{zx} & n\epsilon_{zy} & h_{zz} \end{pmatrix}. \tag{11}$$

In the above equation, ϵ_{ij}'s are the strain tensor components, $\epsilon = \epsilon_{xx} + \epsilon_{yy} + \epsilon_{zz}$, a_c is the conduction band deformation potential, and

$$\begin{aligned} h_{xx} &= l\epsilon_{xx} + m(\epsilon_{yy} + \epsilon_{zz}), \\ h_{yy} &= l\epsilon_{yy} + m(\epsilon_{xx} + \epsilon_{zz}), \\ h_{zz} &= l\epsilon_{zz} + m(\epsilon_{xx} + \epsilon_{yy}). \end{aligned} \tag{12}$$

The parameters l, m, and n can be expressed in terms of valence band deformation potentials, a_v, b, and d as[27]

$$\begin{aligned} l &= a_v + 2b, \\ m &= a_v - b, \\ n &= \sqrt{3}d, \end{aligned} \tag{13}$$

and the components of strain tensor are given by[28]

$$\begin{aligned} \epsilon_{xx} &= \epsilon_{yy} = \frac{a_0 - a}{a}, \\ \epsilon_{zz} &= -\frac{2C_{12}}{C_{11}}\epsilon_{xx}, \\ \epsilon_{xy} &= \epsilon_{yx} = \epsilon_{xz} = \epsilon_{zx} = \epsilon_{yz} = \epsilon_{zy} = 0. \end{aligned} \tag{14}$$

In Eq. (14), a_0 and a are the lattice constants of the substrate and the layer material, respectively, C_{11} and C_{12} are the stiffness constants.

Our theoretical analysis does not include the linear-in-k terms in the Hamiltonian, Kane's B parameter, and the deformation potential b',[29,30] resulting from the lack of inversion symmetry in bulk zinc blende crystals. For the energy interval and the range of in-plane wave vector considered in our work, the neglect of these terms has insignificant effect on the calculated results. The spin-orbit interaction terms in $\hat{H}_\epsilon$ are also ignored,[29,30] because their contribution to the strain-dependent part of the Hamiltonian is small.[27]

III. SOLUTION OF EIGENVALUE PROBLEM

To avoid unphysical spurious solutions,[25] we set $A_c(z) = 0$ and solve the equations for the envelope functions ψ_i

$$\sum_{j=1}^{8} \hat{H}_{ij}\psi_j = E\psi_i, \quad i = 1,2,\ldots,8, \tag{15}$$

where E is an energy, using the scattering matrix method similar to the method in Ref. 23, which allows us to obtain the subband dispersions and wave functions in the structures with thick layers. We first express the conduction band envelope functions, ψ_1 and ψ_5 from the first and fifth equations of Eq. (15) in terms of valence band envelopes as

$$\begin{aligned} \psi_1 &= i(E - E_c - a_c\epsilon)^{-1}P(k_x\psi_2 + k_y\psi_3 + k_z\psi_4), \\ \psi_5 &= i(E - E_c - a_c\epsilon)^{-1}P(k_x\psi_6 + k_y\psi_7 + k_z\psi_8). \end{aligned} \tag{16}$$

Then, substituting the expressions for ψ_1 and ψ_5 into the other six equations of Eq. (15), we arrive at the 6×6 energy-dependent Hamiltonian $\hat{H}^{(e)}$ which describes the evolution of vector $\mathbf{F} = (\psi_2\psi_3\psi_4\psi_6\psi_7\psi_8)^T$ in the following way:

$$\hat{H}^{(e)}\mathbf{F} = E\mathbf{F}. \tag{17}$$

The matrix $\hat{H}^{(e)}$ is obtained from matrix $\hat{H}$ by deleting the conduction band rows and columns and replacing L and N_+ with

$$\begin{aligned} L'(E) &= L + P^2/(E - E_c - a_c\epsilon), \\ N'_+(E) &= N_+ + P^2/(E - E_c - a_c\epsilon). \end{aligned} \tag{18}$$

We find the solution of Eq. (17) in each layer of the structure in terms of plane waves. The wave functions are then matched at the interfaces using the boundary conditions of Burt's envelope function theory. These conditions are obtained by integrating Eq. (17) across the interfaces. As a result, the vector functions $\mathbf{F}$ and $\hat{B}\mathbf{F}$ are required to be continuous, where the 6×6 matrix $\hat{B}$ is

$$\hat{B} = \begin{pmatrix} \hat{B}_3 & 0 \\ 0 & \hat{B}_3 \end{pmatrix}, \tag{19}$$

and the 3×3 block $\hat{B}_3$ is given by

$$\hat{B}_3 = \begin{pmatrix} M\partial/\partial z & 0 & iN_-k_x \\ 0 & M\partial/\partial z & iN_-k_y \\ iN'_+k_x & iN'_+k_y & L'\partial/\partial z \end{pmatrix}. \tag{20}$$

The solution of Eq. (17) in each layer of the quantum well structure can be written as a sum of all transmitted and re-

flected waves having the same energy E and in-plane wave vector (k_x, k_y). For layer n we have

$$\mathbf{F}=\exp(ik_x x+ik_y y)\sum_{j=1}^{6}\{a_j^{(n)}\exp[ik_{z,j}^{(n)}(z-z_{n1})]\mathbf{e}_{+j}^{(n)}+b_j^{(n)}\exp[-ik_{z,j}^{(n)}(z-z_{n2})]\mathbf{e}_{-j}^{(n)}\}. \tag{21}$$

In the above equation, $k_{z,j}$ $(j=1,\ldots,6)$ are the z components of complex wave vectors for the bulk states. All complex wave vectors $k_{z,j}$, which describe the transmitted states, have positive or zero imaginary parts. z_{n1} and z_{n2} are the z coordinates of the left and right boundary of an intermediate layer n. For the left or right barrier layers, we take $z_{n1}=z_{n2}$, where z_{n1} (z_{n2}) is the z coordinate of the AlSb/InAs or GaSb/AlSb interface. In addition, $a_j^{(n)}$ and $b_j^{(n)}$ are the complex coefficients of the transmitted and reflected waves, respectively. The vectors $\mathbf{e}_{+j}^{(n)}$ and $\mathbf{e}_{-j}^{(n)}$ are defined from the equation

$$H^{(e)}(\pm k_{z,j})\mathbf{e}_{\pm j}^{(n)}=E\mathbf{e}_{\pm j}^{(n)}, \tag{22}$$

where the matrices $H^{(e)}(\pm k_{z,j})$ are obtained from matrix $\hat{H}^{(e)}$ by replacing $\hat{k}_z$ with $\pm k_{z,j}$ and $k_{z,j}$ are given by $|H^{(e)}(k_{z,j})-EI|=0$ with I as the unity matrix.

Using the boundary conditions, we match at the interfaces the envelope functions between two neighbor layers. Then the 12×12 scattering matrices $S(m,n)$ defined as

$$\begin{pmatrix}\mathbf{a}^{(n)}\\ \mathbf{b}^{(m)}\end{pmatrix}=S(m,n)\begin{pmatrix}\mathbf{a}^{(m)}\\ \mathbf{b}^{(n)}\end{pmatrix} \tag{23}$$

are calculated as in Ref. 23. In Eq. (23), the vectors $\mathbf{a}^{(n)}$ and $\mathbf{b}^{(n)}$ are the column vectors composed of the coefficients $a_j^{(n)}$ and $b_j^{(n)}$, respectively. Expressing

$$S(m,n)=\begin{pmatrix}S_{11}(m,n) & S_{12}(m,n)\\ S_{21}(m,n) & S_{22}(m,n)\end{pmatrix}, \tag{24}$$

where $S_{ij}(m,n)$ are the 6×6 matrices, the eigenvalue equation can be written as[23]

$$|I-S_{21}(m,N)S_{12}(1,m)|=0. \tag{25}$$

In Eq. (25), index 1 corresponds to the left AlSb barrier, while index N corresponds to the right AlSb barrier, the matrices $S_{ij}(m,n)$ depend on energy E and in-plane wave vector $\mathbf{k}_\parallel$. In deriving this equation, we set the vector coefficients $\mathbf{a}^{(1)}$ and $\mathbf{b}^{(N)}$ for incoming waves to be zero.[23] The vector coefficients $\mathbf{b}^{(m)}$, $\mathbf{a}^{(m)}$, $\mathbf{b}^{(1)}$, and $\mathbf{a}^{(N)}$ are then given by[23]

$$[I-S_{21}(m,N)S_{12}(1,m)]\mathbf{b}^{(m)}=0, \tag{26}$$

$$\mathbf{a}^{(m)}=S_{12}(1,m)\mathbf{b}^{(m)}, \tag{27}$$

$$\mathbf{b}^{(1)}=S_{22}(1,m)\mathbf{b}^{(m)}, \tag{28}$$

$$\mathbf{a}^{(N)}=S_{11}(m,N)\mathbf{a}^{(m)}. \tag{29}$$

IV. RESULTS AND DISCUSSION

For the calculation of the electronic band structures, we take the parameters (energy gaps, split-off energies, Luttinger parameters, interband momentum matrix elements, lattice constants for different layer materials, conduction and valence band discontinuities for the unstrained heterojunctions) from Ref. 22. The modified Luttinger parameters are calculated as in Ref. 25. The deformation potential constants and the stiffness constants are obtained from Ref. 31. The lattice-mismatched strain causes the shift of the conduction and valence band edges and the split of the bulk zone center light-hole and heavy-hole levels,[28–30] yielding different band offsets of the light-hole and heavy-hole bands. The strain also changes the electron and hole bulk dispersions near the band edges. This results in the modification of subband dispersions.

The electronic band structures for the quantum well structure with a 10 nm InAs layer and a 10 nm GaSb layer are shown in Fig. 2, where panel (a) is for the unstrained quantum well structure, panel (b) is for the strained structure grown on InAs, and panel (c) corresponds to the strained quantum well grown on GaSb. There are five subbands in each panel of Fig. 2, which are labeled $1e$ for electrons, $1lh$ for light holes, and $1hh$, $2hh$, $3hh$ for heavy holes. (We assumed that $E=0$ at the conduction band edge of unstrained InAs.) The label for a subband corresponds to its wave function property at the zone center. To assign the labels to different subbands, we plot the occupation probabilities ($|\psi|^2=\Sigma_{i=1}^{8}|\psi_i|^2$) at $\mathbf{k}_\parallel=0$ of these five subbands of interest in Fig. 3, where panels (a), (b), and (c) are for the same cases as in Fig. 2. For convenience, the wave functions in Fig. 3 are shifted up according to the values of energies of the corresponding levels. Hence, the flat parts of each curve in Fig. 3 imply the zero occupation probability. The wave functions of the heavy-hole states $1hh$, $2hh$, and $3hh$ are localized in the GaSb layer because of the absence of interaction with the electron and light-hole states at $\mathbf{k}_\parallel=0$. On the other hand, the hybridization of the $1e$ and $1lh$ states occurs even at the zone center. In this case, we assign label $1e$ $(1lh)$ to the subband if its wave function at $\mathbf{k}_\parallel=0$ is localized mainly in the InAs (GaSb) layer.

Shown in Fig. 2 are the subband dispersions along different $\mathbf{k}_\parallel$ directions. At $\mathbf{k}_\parallel\neq 0$ the spin-degeneracy breaks, and considerable spin-splitting of subbands can be seen in each panel of Fig. 2 along both [10] and [11] directions. Especially great spin-splitting undergoes the $1lh$ subband in panel (c) around the highest minigap. At the same time only weak subband anisotropy exists in this quantum well for the considered values of E and $\mathbf{k}_\parallel$, while larger anisotropy will be obtained for the structure with the thicker InAs layer. Only $1hh$ level is above the $1e$ level at $\mathbf{k}_\parallel=0$ in Fig. 2(a). Taking the strain into account, we obtain that the $1hh$ and $2hh$ levels are higher than the $1e$ level in the structure grown on InAs, while the three levels ($1hh$, $1lh$, and $2hh$) lie above the $1e$ level in the one grown on GaSb. The highest minigap moves away from the zone center in Figs. 2(b) and 2(c) due to the lattice mismatched strain. In addition the highest hybridization gap magnitudes for the well grown on

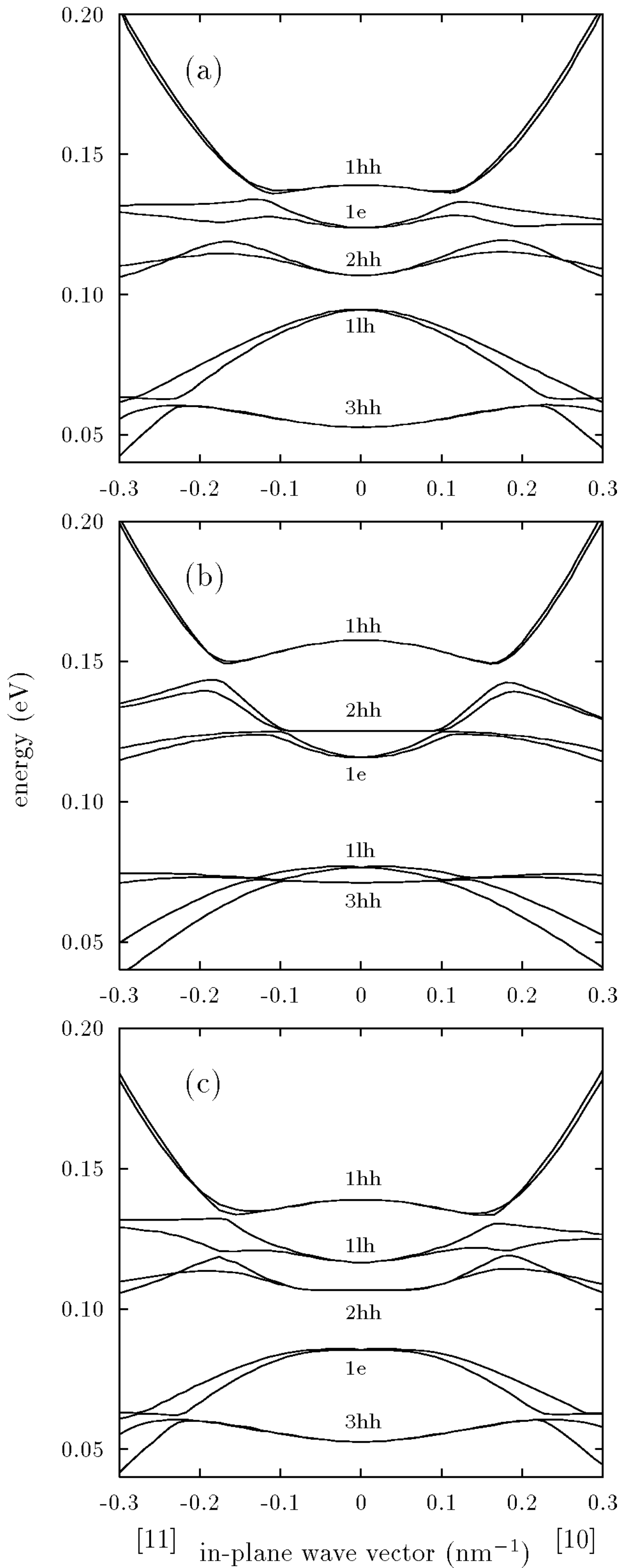

FIG. 2. Electronic band structures for the quantum well structure with a 10 nm InAs and a 10 nm GaSb.

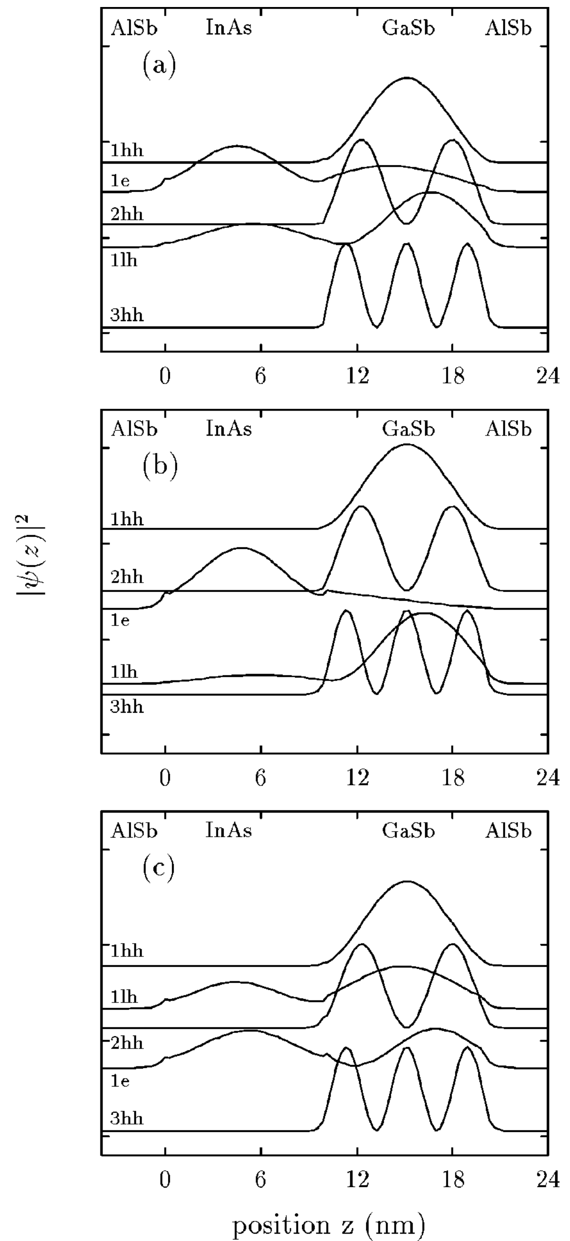

FIG. 3. Normalized probability density $|\psi(z)|^2$ for the zone center states in a quantum well with a 10 nm InAs layer and a 10 nm GaSb layer.

InAs in Fig. 2(b) are considerably greater than those in Figs. 2(a) and 2(c). In Fig. 2(c), it can be found that a wide hybridization gap also occurs at $\mathbf{k}_{\parallel}\approx 0$ between $1lh$ and $1e$ subbands. The wave functions of the two subbands [see Fig. 3(c)] are strongly mixing in comparison with those shown in Figs. 3(a) and 3(b). With moving away from the zone center, the $1e$ subband becomes light-hole-like, while the $1lh$ subband becomes electronlike. The wave function behavior around the anticrossing gaps has been considered in detail in Refs. 17,23.

As the InAs layer of the structure becomes thicker, the hybridization gap between the highest heavy-hole-like subband and the lowest electronlike subband decreases. This can be clearly seen from Fig. 4, where we plot the subband dispersions for the structure with a 15 nm InAs layer and a 10 nm GaSb layer. (This structure was investigated experimentally in Ref. 7.) The panels (a), (b), and (c) in Fig. 4 are

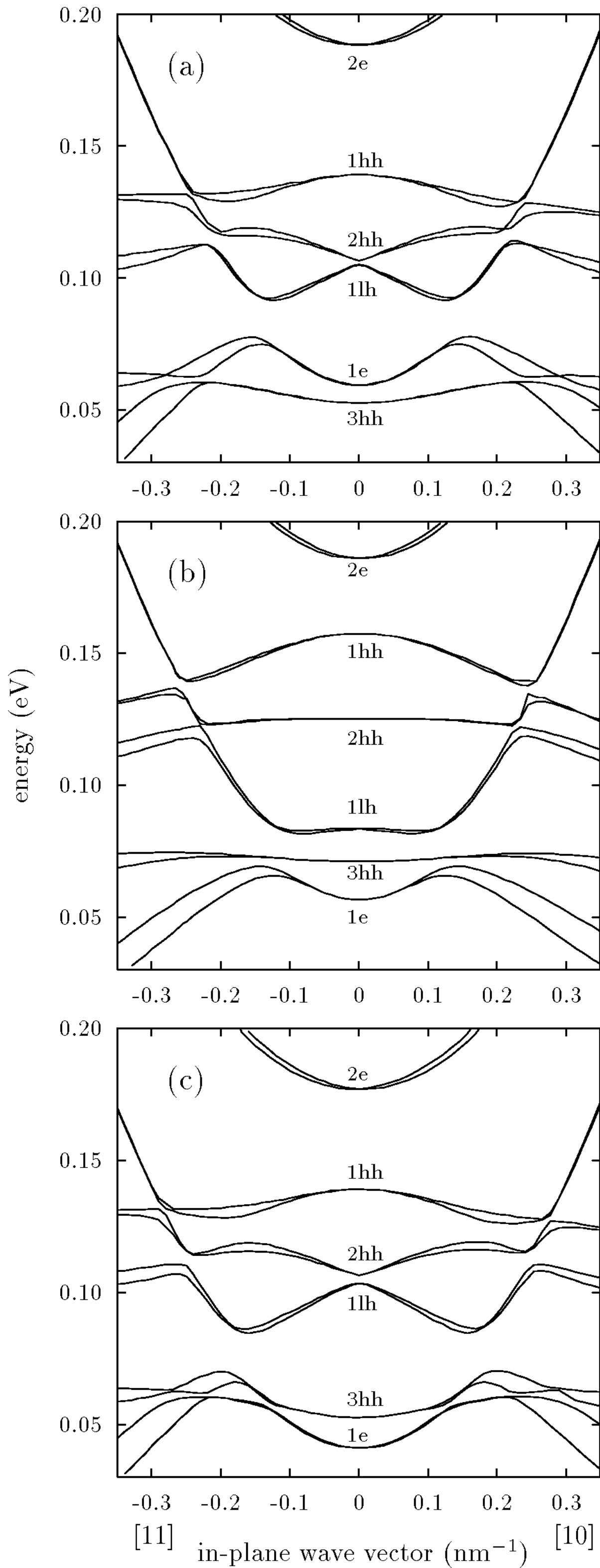

FIG. 4. Electronic band structures for the quantum well structure with a 15 nm InAs and a 10 nm GaSb.

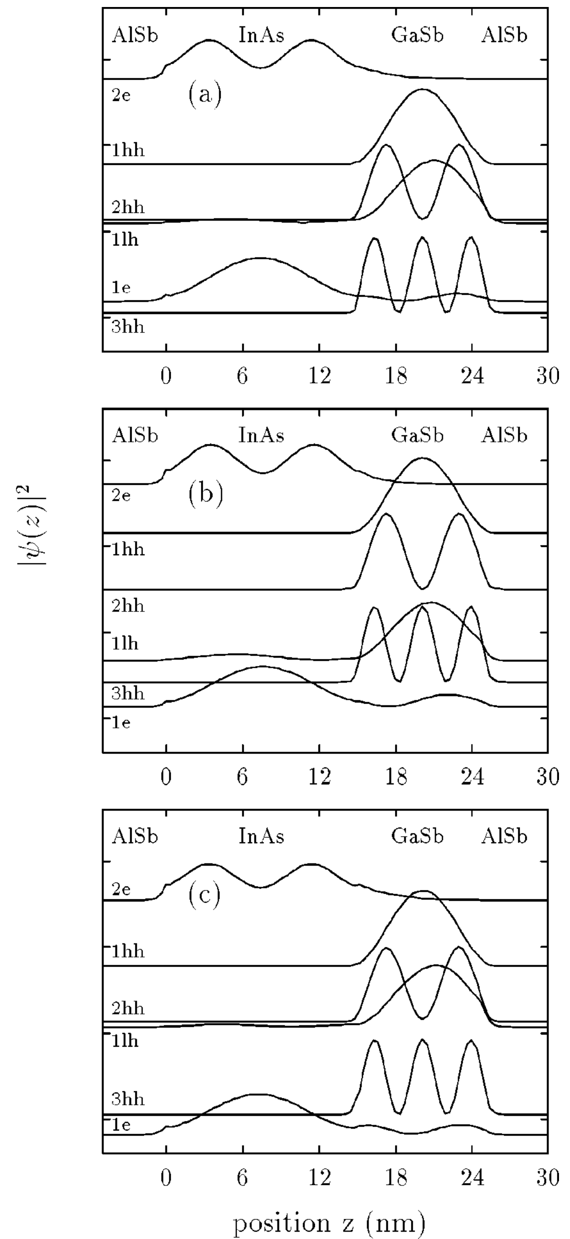

FIG. 5. Normalized probability density $|\psi_{(z)}|^2$ for the zone center states in a quantum well with a 15 nm InAs layer and a 10 nm GaSb layer.

similar to those in Fig. 2. Six subbands are shown in each panel of Fig. 4, which are labeled according to the spatial distribution of the corresponding occupation probabilities presented in Fig. 5. The $1e$ level is the lowest one at $\mathbf{k}_{\parallel}=0$ for the strained structure grown either on InAs [panel (b) in Fig. 4] or on GaSb [panel (c) in Fig. 4]. However, the calculation performed neglecting the strain [see panel (a) in Fig. 4] gives the $3hh$ level lower than the $1e$ level. With the in-plane wave vector increasing, the electronlike subband anticrosses sequentially with the $1lh$, $2hh$, and $1hh$ subbands as shown in Figs. 4(a) and 4(b), and with the $3hh$, $1lh$, $2hh$, and $1hh$ subbands as shown in Fig. 4(c). This results in multiple minigaps. In Fig. 4(b), which is for the structure grown on InAs, the $3hh$ subband lies inside the wide hybridization gap between the electronlike ($1e$) and light-hole-like ($1lh$) subbands and remains almost unperturbed. Similar wide minigaps between the electronlike ($3hh$) and light-

holelike ($1lh$) subbands in the in-plane dispersion of the structure grown on GaSb occur at larger values of $k_{\parallel}$.

Here we discover an interesting effect which can be treated as strain-induced semimetal-semiconductor phase transition. Let us consider the in-plane dispersions in the vicinity of the highest hybridization minigaps in Fig. 4. Comparing the electronic band structures in panels (b) and (c) with that in panel (a), we conclude that the gap positions in k space considerably enlarge because of the lattice-mismatched strain as in the structure with a 10 nm InAs layer. In addition, the subband anisotropy becomes more noticeable around the hybridization gaps in this figure. Due to the spin-splitting of subbands, the minigaps in the different $\mathbf{k}_{\parallel}$ directions are negative and indirect as can be found in Fig. 4(a), where strain effects are neglected. Similar indirect negative minigaps exist in the electronic band structure of the quantum well grown on GaSb [see Fig. 4(c)]. This structure can exhibit a semimetallic property. This means that electrons in the lowest conduction-band-like subband (the $1hh$ subband around the anticrossing point) can coexist with the holes in the highest valence-band-like subband (the $2hh$ subband). In the structure grown on InAs, the GaSb layer is strained instead of InAs layer. This difference leads to quite different band structures. Positive and direct hybridization gaps in Fig. 4(b) result in a semiconducting behavior. Such a strain-induced phase transition can be observed experimentally by means of measurements of electron and hole concentrations in the InAs/GaSb quantum wells grown on different substrates.

V. CONCLUSION

We have presented a study of the hybridized electron-hole in-plane dispersions in strained AlSb/InAs/GaSb/AlSb quantum well structures, based on the eight-band $\mathbf{k}\cdot\mathbf{p}$ model and the scattering matrix method. The quantum wells grown on InAs and on GaSb have been considered. The difference in lattice-mismatch strain leads to the difference in order of the levels at the zone center and in the subband dispersions. The positions and magnitudes of the hybridization gaps between the electronlike and holelike subbands are sensitive to the lattice-mismatched strain. The spin-splitting of subbands is also strain dependent. Due to the large spin splitting of subbands, the hybridization gaps between the electronlike subband and the highest heavy-hole-like subband along different directions of in-plane wave vector, which have been observed experimentally, are smaller in the structure grown on GaSb than those in the structure grown on InAs. These gaps have been found to be negative and indirect in the structure with a thick 15 nm InAs layer and a 10 nm GaSb layer grown on GaSb. Since electrons in the lowest conduction-band-like subband can coexist with holes in the highest valence-band-like subband, this structure is in a semimetal phase. On the other hand, the small spin splitting of subbands around the highest hybridization gap in a similar structure grown on InAs results in a positive and direct gap. This structure is therefore in a semiconductor phase with a small hybridization gap. Semimetal-semiconductor phase transition can hence be induced by the lattice-mismatched strain.

[1] G.A. Sai-Halasz, L. Esaki, and W.A. Harrison, Phys. Rev. B **18**, 2812 (1978).

[2] M. Altarelli, Phys. Rev. B **28**, 842 (1983).

[3] M.J. Yang, C.H. Yang, B.R. Bennett, and B.V. Shanabrook, Phys. Rev. Lett. **78**, 4613 (1997).

[4] L.J. Cooper, N.K. Patel, V. Drouot, E.H. Linfield, D.A. Ritchie, and M. Pepper, Phys. Rev. B **57**, 11 915 (1998).

[5] M. Lakrimi, S. Khym, R.J. Nicholas, D.M. Symons, F.M. Peeters, N.J. Mason, and P.J. Walker, Phys. Rev. Lett. **79**, 3034 (1997).

[6] A.J.L. Poulter, M. Lakrimi, R.J. Nicholas, N.J. Mason, and P.J. Walker, Phys. Rev. B **60**, 1884 (1999).

[7] T.P. Marlow, L.J. Cooper, D.D. Arnone, N.K. Patel, D.M. Whittaker, E.H. Linfield, D.A. Ritchie, and M. Pepper, Phys. Rev. Lett. **82**, 2362 (1999).

[8] L.L. Chang, J. Phys. Soc. Jpn. Suppl. **49**, 997 (1980).

[9] Y. Guldner, J.P. Vieren, P. Voisin, M. Voos, L.L. Chang, and L. Esaki, Phys. Rev. Lett. **45**, 1719 (1980).

[10] S.R. White and L.J. Sham, Phys. Rev. Lett. **47**, 879 (1981).

[11] J.C. Maan, Y. Guldner, J.P. Vieren, P. Voisin, M. Voos, L.L. Chang, and L. Esaki, Solid State Commun. **39**, 683 (1981).

[12] L.L. Chang, N.J. Kawai, G.A. Sai-Halasz, R. Ludeke, and L. Esaki, Appl. Phys. Lett. **35**, 939 (1979).

[13] A. Fasolino and M. Altarelli, Surf. Sci. **142**, 322 (1984).

[14] M. Altarelli, J.C. Maan, L.L. Chang, and L. Esaki, Phys. Rev. B **35**, 9867 (1987).

[15] Yu. Vasilyev, S. Suchalkin, K. von Klitzing, B. Meltser, S. Ivanov, and P. Kop'ev, Phys. Rev. B **60**, 10 636 (1999).

[16] L.-W. Wang, S.H. Wei, T. Mattila, A. Zunger, I. Vurgaftman, and J.R. Meyer, Phys. Rev. B **60**, 5590 (1999).

[17] R. Magri, L.W. Wang, A. Zunger, I. Vurgaftman, and J.R. Meyer, Phys. Rev. B **61**, 10 235 (2000).

[18] Y. Noveh and B. Laikhtman, Appl. Phys. Lett. **66**, 1980 (1995).

[19] J.C. Chiang, S.F. Tsay, Z.M. Chau, and I. Lo, Phys. Rev. Lett. **77**, 2053 (1996).

[20] J.J. Quinn and J.J. Quinn, Surf. Sci. **361**, 930 (1996).

[21] S. de-Leon, L.D. Shvartsman, and B. Laikhtman, Phys. Rev. B **60**, 1861 (1999).

[22] E. Halvorsen, Y. Galperin, and K.A. Chao, Phys. Rev. B **61**, 16 743 (2000).

[23] A. Zakharova, S.T. Yen, and K.A. Chao, Phys. Rev. B **64**, 235332 (2001).

[24] M.G. Burt, J. Phys.: Condens. Matter **4**, 6651 (1992).

[25] B.A. Foreman, Phys. Rev. B **56**, R12 748 (1997).

[26] D.Y.K. Ko and J.C. Inkson, Phys. Rev. B **38**, 9945 (1988).

[27] G.L. Bir, G.E. Pikus, *Symmetry and Strain-Induced Effects in Semiconductors* (Wiley, New York, 1974).

[28] C.Y.-P. Chao and S.L. Chaung, Phys. Rev. B **46**, 4110 (1992).

[29] T.B. Bahder, Phys. Rev. B **41**, 11992 (1990); **46**, 9913 (1992).

[30] T.B. Bahder, Phys. Rev. B **45**, 1629 (1992).

[31] M.P.C.M. Krijn, Semicond. Sci. Technol. **6**, 27 (1991).